The influence of lattice termination on the edge states of the quantum spin Hall insulator monolayer $1T'$-WTe_2: Supplemental Material

Alexander Lau,[1] Rajyavardhan Ray,[2,3] Dániel Varjas,[1,4] and Anton Akhmerov[1]

[1] *Kavli Institute of Nanoscience, Delft University of Technology, P.O. Box 4056, 2600 GA Delft, Netherlands*
[2] *Institute for Theoretical Solid State Physics, IFW Dresden, Helmholtzstr. 20, 01069 Dresden, Germany*
[3] *Dresden Center for Computational Materials Science (DCMS), TU Dresden, 01062 Dresden, Germany*
[4] *QuTech, Delft University of Technology, P.O. Box 4056, 2600 GA Delft, The Netherlands*

(Dated: May 8, 2019)

A. DETAILS OF MODEL CONSTRUCTION

In the main text, we construct a minimal 4-orbital tight-binding model for monolayer WTe_2. In the following, we provide more details on the single steps of the construction.

A.1. DFT calculations and optimized Wannier-orbital fit

First of all, to capture the essential features of the scalar-relativistic density-functional theory (DFT) band-structure at low energies, we have to include a large number of neighbors in the Wannier-orbital fit (hopping range up to 20 Å). Irrespective of the number of neighbors in the low-energy model, however, the location of the Dirac point in **k** space is slightly shifted compared to the DFT band structure. While a more complex 6-orbital model does not suffer from such discrepancies, also within the minimal 4-orbital model we obtain an accurate low-energy description by adopting the hybrid approach described below.

First, we systematically reduce the number of neighbors by introducing a cut-off, keeping only hopping terms with magnitude larger than or equal to 0.06 eV. In addition, we include second-nearest neighbor hopping t_{py} in the y-direction, which is slightly smaller than the cuf-off. This is necessary to avoid a nearly flat dispersion of the highest valence band along the Γ–Y direction, since t_{py} has a dominant contribution to the finite curvature along this line. Next, we fix the onsite energies and all dominant hopping parameters ≥ 0.40 eV. We treat the remaining parameters as effective to account for neglected longer-range hopping terms and for the discrepancies between the Wannier model and the band structure mentioned above.

We then fit the effective parameters to the DFT energy bands close to the Fermi level to capture accurately the low-energy details of the band structure. To keep the deviations small and to reduce the number of model parameters further, we employ a LASSO regression analysis with a regularization parameter λ. We determine the optimal λ such that the modified model parameters are close to their original values, with the largest change equal to 0.17 eV, and such that they are all smaller than the dominant hopping parameters. Finally, we discard the parameters smaller than the cut-off value.

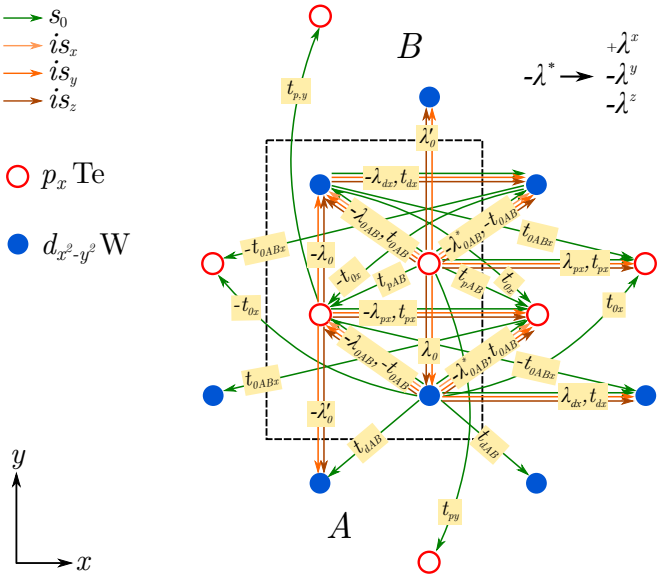

Figure S.1. Cartoon of hopping and symmetry-allowed SOC terms.

A.2. Fitting SOC parameters to ARPES data

We now add all symmetry-allowed spin-orbit coupling (SOC) terms up to nearest neighbors to our model. Furthermore, we also add symmetry-allowed, next-nearest neighbor SOC terms in the x direction. We expect those to be non-negligible since the parameters of the related hopping terms t_{px} and t_{dx} are among the largest in the spinless Hamiltonian (see Tab. 1 in the main text). The SOC terms are illustrated in Fig. S.1. To determine the corresponding SOC parameters, we choose to fit these parameters to experimental data from angle-resolved photoemission spectroscopy (ARPES) close to the Fermi level. The raw data has been provided by the authors of Ref. 1.

The raw data comprises measured ARPES spectra of monolayer WTe_2 along three different directions through the two-dimensional Brillouin zone, namely along ΓX, along ΓY, and along ΓM. Furthermore, we also use ARPES raw data for K-doped monolayer WTe_2 along

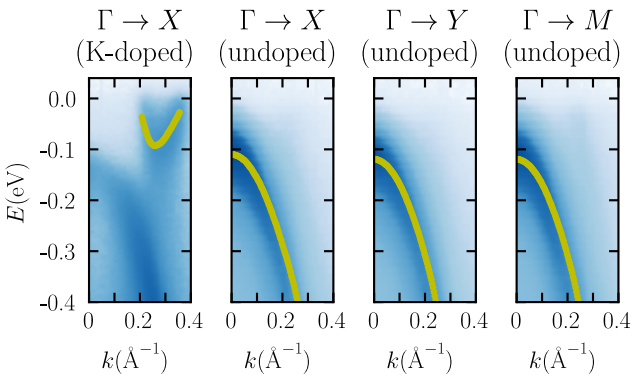

Figure S.2. ARPES spectra (blue) from Ref. 1 close to the Fermi level and overlaid intensity peaks (yellow).

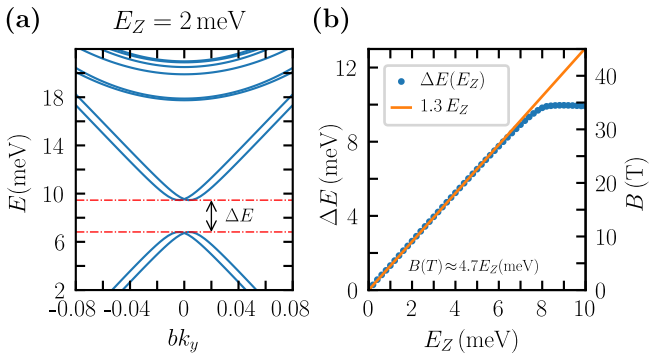

Figure S.3. Edge energy gap for sawtooth y-ribbons under magnetic field: (a) magnified ribbon spectrum around the edge energy gap ΔE, which we have indicated by red, dash-dot lines. (b) Edge energy gap ΔE and magnetic field B as a function of the Zeeman energy E_Z.

ΓX, for which the Fermi level lies in the conduction band. From the raw data we determine the peaks of the spectral weights by fitting to ensembles of Lorentzians. In this way, we obtain experimental energy bands for the first valence band close to Γ along three different directions, and for a small piece of the first conduction band along ΓX (see Fig. S.2). The distance in energy between the valence and the conduction bands is set to the value of 56 meV, obtained from scanning tunneling spectroscopy (STS) measurements on the same samples in Ref. 1.

Besides a good agreement with the ARPES peaks for the individual energy bands, we require the induced indirect energy gap to equal the STS value. To account for discrepancies between ARPES data and DFT, we further allow for small perturbations of the two smallest hopping parameters t_{py} and t_{0x}, which we obtained above for the tight-binding model without SOC. To handle the large number of free parameters, we again employ a LASSO regression analysis. We choose the optimal regularization parameter such that the model has an energy gap identical to the STS value and such that the perturbations of the spinless parameters are $\leq 0.02\,\mathrm{eV}$. Finally, we discard SOC parameters $< 8\,\mathrm{meV}$, which does not affect the quality of the fit result considerably.

A.3. The final tight-binding model

The schematic in Fig. S.1 illustrates the hopping and SOC terms with their corresponding parameters. Based on this, the full tight-binding model given in the main text can be assembled by making use of translational symmetry and Hermiticity only. Relations between terms connected by other symmetries are captured by the notation.

In the main text, we also provide the corresponding Bloch Hamiltonian $H(\mathbf{k}) = H_0(\mathbf{k}) + H_{SOC}(\mathbf{k})$. There, we introduce the 4×4 matrices Γ_i defined by:

$$\Gamma_0 = \tau_0\sigma_0, \tag{1}$$
$$\Gamma_1^{\pm} = \frac{\tau_0}{2}(\sigma_0 \pm \sigma_3), \tag{2}$$
$$\Gamma_2^{\pm} = \frac{1}{4}(\tau_1 + i\tau_2)(\sigma_0 \pm \sigma_3), \tag{3}$$
$$\Gamma_3 = \frac{1}{2}(\tau_1 + i\tau_2)i\sigma_2, \tag{4}$$
$$\Gamma_4^{\pm} = \frac{1}{4}(\tau_0 \pm \tau_3)(\sigma_1 + i\sigma_2), \tag{5}$$
$$\Gamma_5^{\pm} = \frac{\tau_3}{2}(\sigma_0 \pm \sigma_3), \tag{6}$$
$$\Gamma_6 = \frac{1}{2}(\tau_1 + i\tau_2)\sigma_1, \tag{7}$$

where the matrices $\tau_j\sigma_i$ are products of Pauli matrices acting in orbital space with respect to the basis $\{d_{\mathbf{k}Ads}, d_{\mathbf{k}Aps}, d_{\mathbf{k}Bds}, d_{\mathbf{k}Bps}\}$, where $d_{\mathbf{k}cls}$ annihilates an electron with momentum $\mathbf{k}$, spin-S_z eigenvalue $s = \uparrow, \downarrow$ and orbital $l = p, d$ (Te,W) in sublattice $c = A, B$. More specifically, τ_j acts on the sublattice degree of freedom and σ_i acts on the orbital degree of freedom.

B. DETERMINING THE MAGNETIC FIELD FROM THE EDGE GAP

In the main text, we study the effect of an onsite Zeeman term in the Hamiltonian of monolayer WTe_2 on the edge dispersion of differently terminated ribbons. Since it breaks time-reversal symmetry, it gaps out the edge Dirac points in the ribbon spectrum, if present. If the edge Dirac point lies inside the energy gap of the bulk bands, the Zeeman term thus opens a direct energy gap in the spectrum of the ribbon. In particular, we have seen that y-ribbons with a sawtooth termination realize this edge Zeeman gap. Figure S.3(a) shows a magnified region of the ribbon spectrum around the edge gap.

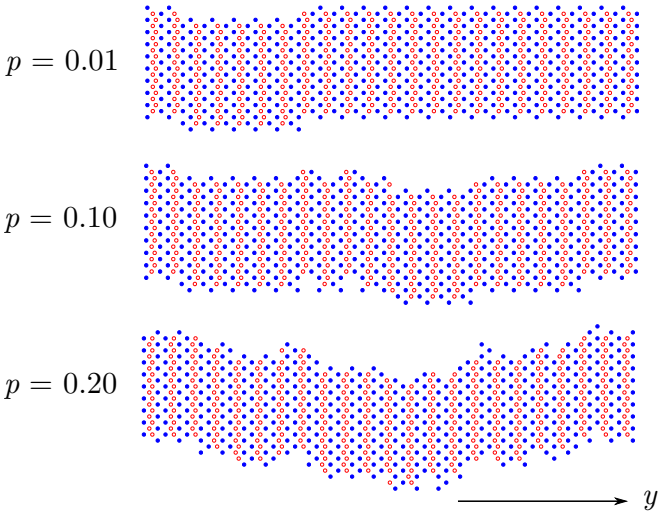

Figure S.4. Geometries of sawtooth y-ribbons with disordered edge terminations as a function of the disorder parameter p.

We now use the size of the observed edge Zeeman gap ΔE to determine the relation between the magnetic field $\mathbf{B} = B\mathbf{e}_z$ and the Zeeman energy E_Z. For that purpose, we make use of the relation

$$\Delta E = g\mu_B B, \tag{8}$$

where μ_B is the Bohr magneton and g is the effective out-of-plane g factor. A recent experiment[2] has observed an edge Zeeman gap in WTe_2 monolayers and has obtained a value of $g = 4.8$.

We have computed ribbon spectra for a number of values for the Zeeman energy E_Z and determined the size of the induced Zeeman gap ΔE for each realization [see Fig. S.3(a)]. We plot the results in Fig S.3(b), where we have also added a second axis to indicate the corresponding magnetic field B based on Eq. (8) and on the experimental g factor. We find that the relation between E_Z and B is approximately linear for small values of E_Z. More specifically, we determine the linear relation to be

$$B[\mathrm{T}] = 4.7\, E_Z[\mathrm{meV}]. \tag{9}$$

At large magnetic fields, the growing edge gap is compensated by the shrinking bulk gap of the system.

C. MODELING OF DISORDERED RIBBONS

We model disordered (or rough) edges by adding and removing lattice sites along an initial, translationally invariant boundary following a random walk $x_p(y)$ with parameter p and step widths Δx and Δy. More specifically, a step by Δy in the variable y is accompanied by either a step of $+\Delta x$ in the variable x with probability $p/2$, a step of $-\Delta x$ in x with probability $p/2$, or no step in x with probability $1 - p$.

Starting from translationally invariant y-ribbons with sawtooth terminations, as done in the main text, we choose the step lengths in the following way: a step Δy in the random walk corresponds to a step by one lattice site parallelly along the sawteeth, whereas a step Δx in the random walk converts to a step by one lattice site in the x direction. In particular, we choose $\Delta y = b/4$ and $\Delta x = a$. Furthermore, without loss of generality, we choose the initial and the final point of the random walk to be the same, i.e., $x_p(y_0) = x_p(y_0 + N\Delta y)$, where N is the length of the random walk.

In Fig. S.4 we show realizations of ribbons, subject to the prescription above, for different values of the disorder strength p. For small p, the edge is very unlikely to deviate from the initial sawtooth termination and we see long, non-disordered segments separated by steps. For larger p, however, deviations from the initial, clean edge become dominant.

D. LIMITATIONS OF THE NANORIBBON MODELS

In the main text, we model finite nanoribbon geometries by truncating the real-space bulk Hamiltonian. As a reasonable starting point, this is expected to give a qualitative picture of the effects of such lattice terminations but comes with limitations.

In general, the edge resulting from the termination of a material is chemically active due to the presence of dangling bonds. Depending on the experimental setup, this will lead to passivation with other atoms, such as oxygen or hydrogen. In WTe_2 monolayers, which are encapsulated in boron nitride,[2] such passivation is expected to involve boron and nitride. However, the detailed effects of such an environment on the edges of WTe_2 monolayers are not known.

On the level of a low-energy model, such effects will mainly induce effective edge potentials that deform the edge-energy bands associated with a specific termination. In particular, such potentials can shift the edge Dirac points energetically. If the edge potentials are strong enough, this can push an edge Dirac point out of the bulk-energy gap or vice versa. Moreover, edge potentials can lead to additional trivial edge bands lurking into the bulk-energy gap. If the edge potentials are small, they will have only a perturbative effect on the edge dispersions obtained from the truncated bulk model. Nonetheless, all of the effects above can be easily incorporated into the truncated bulk model once the induced edge potentials are known from experiments or from sufficiently accurate *ab-initio* studies of nanoribbons.

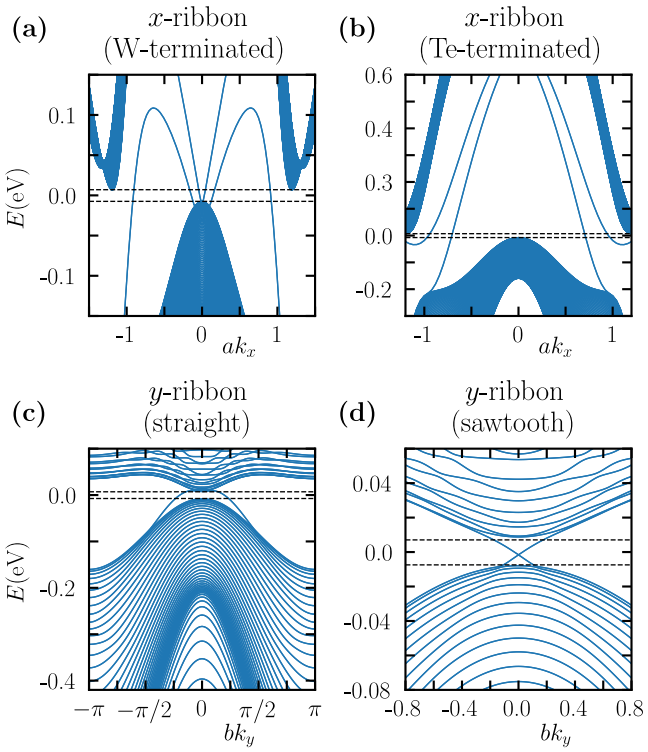

Figure S.5. Edge spectra with original Wannier bulk parameters without magnetic field for the same ribbon geometries as shown in the main text. The dashed lines indicate the edges of the bulk valence and bulk conduction bands, respectively.

E. EFFECT OF BULK-PARAMETER PERTURBATIONS ON THE EDGE DISPERSIONS

In the main text, we optimize the spinless hopping parameters to obtain a low-energy bulk model with an accurate dispersion close to the Fermi level. This results in a small deviation of the original Wannier parameters obtained from an optimization of the orbital overlaps. In the following, we are going to show that this deviation has only a small quantitative effect on the edge dispersion of corresponding nanoribbons.

For that, we use all Wannier parameters with a magnitude larger than or equal to 0.06 eV plus the original second-nearest neighbor hopping t_{py} in the y direction. Furthermore, we apply the SOC parameters of the final model. The edge spectra of nanoribbons with this set of bulk parameters are shown in Fig. S.5, where the panels correspond to the same terminations as in the main text.

First of all, we find that the bulk-energy gap, induced by the SOC terms, is much smaller than in the optimized model, namely 14 meV instead of 56 meV. This is due to the large deviation of the spinless Wannier model from the DFT energy bands close to the Fermi level, which underlines the need for optimization. More specifically, the bulk Dirac point is much lower in energy with respect to the band maximum at Γ, while being at a momentum farther away from Γ than in DFT (see Fig. 2 in the main text). This discrepancy would require the SOC terms to be unphysically scaled up (by a factor of 1.3) to achieve the experimentally observed bulk-energy gap. In other words, the SOC gap at the Dirac points would be largely overestimated without optimizing the spinless bands close to the Fermi level.

Similar to the bulk bands, the edge bands are deformed by this parameter perturbation. Nevertheless, their qualitative features remain the same: only the saw-tooth termination in Fig. S.5(d) features an in-gap edge Dirac point, whereas the Dirac points are buried for the other terminations. Furthermore, also the relative location of the buried Dirac points is unchanged, i.e., whether they are buried in the bulk valence or bulk conduction band. This suggests that these features are robust towards mild perturbations of the tight-binding parameters.

[1] S. Tang *et al.*, *Quantum spin Hall state in monolayer 1T′-WTe₂*, Nat. Phys. **13**, 683 (2017).
[2] S. Wu *et al.*, *Observation of the quantum spin Hall effect up to 100 Kelvin in a monolayer crystal*, Science **359**, 76 (2018).